Mitigating Elevation-Dependent Errors in Tropospheric Delay Interpolation for InSAR Applications

Ehsan Nekouzade Chaharmahali *, Jamal Asgari

Department of Geomatics Engineering, Faculty of Civil Engineering and Transportation, University of Isfahan, Iran - nekouzade@gmail.com, asgari@eng.ui.ac.ir

Keywords: Tropospheric delay interpolation, InSAR corrections, Zenith tropospheric delay, ZTD Interpolation

Abstract

Interferometric Synthetic Aperture Radar (InSAR) is a powerful tool for detecting ground deformation with millimeter precision. However, atmospheric effects, particularly tropospheric delays, significantly degrade the accuracy of InSAR-derived measurements. This study investigates elevation-dependent errors in tropospheric delay interpolation using Global Navigation Satellite System (GNSS)-derived Zenith Tropospheric Delay (ZTD) data. Two GNSS networks with similar spatial configurations but different elevation characteristics were analyzed to quantify the effect of altitude differences on interpolation accuracy. A novel correction method was proposed to mitigate the elevation-induced bias by isolating and modifying the dry component of the ZTD using the Saastamoinen model. Results demonstrate that this approach substantially improves interpolation accuracy up to 92% enhancement in high-relief areas. The findings highlight the critical importance of considering elevation effects when integrating GNSS and InSAR data for atmospheric delay correction, especially in mountainous regions.

1. Introduction

Interferometric Synthetic Aperture Radar (InSAR) provides millimeter-level measurements of ground surface deformation. Nowadays this technique is used for different applications such as earthquakes (e.g., Bell et al., 2012; Feng et al., 2010; Jónsson, 2008; Jónsson et al., 2003; Massonnet et al., 1993; Simons et al., 2002), volcanic activity (e.g., Amelung et al., 2007; Plattner et al., 2013; Rivera et al., 2017; Ruch et al., 2016; Sigmundsson et al., 2010), slow tectonic movements (e.g., Cavalié & Jónsson, 2014; Elliott et al., 2008; Walters et al., 2013; Wright et al., 2004), and extraction of the subsurface fluids and mineral resources (e.g., Bawden et al., 2001; Liu et al., 2016; Yang et al., 2017). however, InSAR observations are strongly affected by atmospheric conditions, particularly tropospheric delay. Troposphere effects on InSAR observations can be corrected using different approaches. These corrections can be divided into three groups: i) empirical, ii) statistical, and iii) predictive corrections (Cao et al., 2021). Empirical corrections try to reduce the tropospheric effects by modelling the relationship between topographic height and InSAR phase values (Bekaert, et al., 2015a; Lin et al., 2010; Wicks, 2002). These methods can be quite successful but do not work well when atmospheric turbulence dominates the tropospheric effects (Liang et al., 2018) and can be troublesome when the deformation is correlated with topography (Delacourt et al., 1998). The second category of corrections aims to mitigate tropospheric delays based on time-series of SAR images or interferograms by using statistical, geo-statistical, or adjustment algorithms, such as stacking (Sandwell and Sichoix, 2000), a range of least-squares-based methods with an empirical deformation model (Berardino et al., 2002; Cao et al., 2017; Li et al., 2019), or spatio-temporal filtering (Cao et al., 2019; Ferretti et al., 2001; Hooper, 2008). Unfortunately, statistical approaches are usually not very effective as they rely on averaging stochastic properties of the spatio-temporal tropospheric delays and normally require a large number of SAR images for obtaining satisfactory results (Cao et al., 2017; Siddique et al., 2018). The third group of methods, predictive corrections, use auxiliary atmospheric datasets to compute and correct the InSAR tropospheric delays. Numerous algorithms have been presented that either use one type or multiple different external atmospheric information from local meteorological data (Li et al., 2004), GNSS measurements (Houlie et al., 2016; Onn and Zebker, 2006; Webley et al., 2002), satellite-based multispectral observations from MERIS (MEdium Resolution Imaging Spectrometer onboard ENVISAT satellite) (Li et al., 2009, 2012) and MODIS (MODerate resolution Imaging Spectrometer onboard Terra and Aqua satellites) (Li, 2005), and weather models (Doin et al., 2009; Foster et al., 2006; Hobiger et al., 2010; Jolivet, Grandin, et al., 2011; Liu et al., 2009; Wadge et al., 2002). Spectrometer measurements require collocated sensors and cloud-free conditions and only available in daytime. Time differences between radar and Precipitable Water Vapor (PWV) data can be regarded as limitation. Moreover, the Spectrometer cannot estimate the atmosphere's dry component and calculate the wet part of the delay (Bekaert, et al., 2015b). for the numerical weather models such as ERA5 (calculated by the European Center for Medium-Range Weather Forecasting), The low spatial resolution and the original mismatch in time between the model and the SAR acquisition do not permit addressing the turbulent component that takes place at lower Spatio-temporal scales. Moreover, complex data processing can be regarded as disadvantage of this method (Fattahi and Amelung, 2015). Given the disadvantages mentioned for these methods, using interpolated zenith tropospheric delay (ZTD) values derived from GNSS networks, can be a more accurate strategy to correct InSAR observations (Onn and Zebker, 2006). Because ZTD is strongly dependent on altitude, significant elevation differences between GNSS receivers and the study area can reduce interpolation accuracy. To evaluate this effect, in the third section we compared interpolation accuracy in two GNSS networks with similar

* Corresponding author

configurations (four surrounding receivers and one central receiver) but different elevation characteristics. In the second section we give some information about the networks structure and in the fifth section, we applied a new algorithm that integrates a physical model to account for elevation effects. This algorithm improves the interpolation accuracy in both networks.

2. Case Studies

The case studies we are investigating are two networks with similar configurations but different elevation characteristics. In both of the networks, we have a central receiver that is surrounded with four other receivers. The mean elevation difference between the central and surrounding stations is 122 m in the first network and 1095 m in the second. The locations of the networks and the receiver heights are shown in Figures 1 and 2.

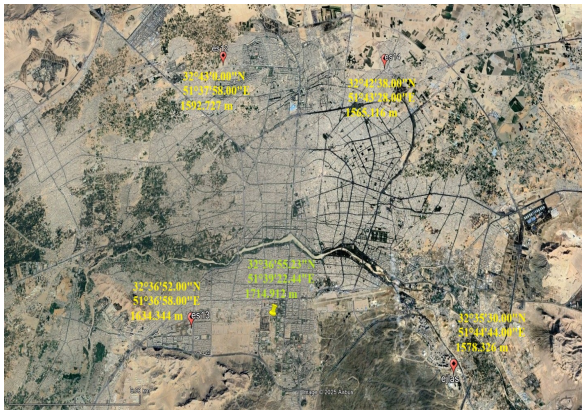

Figure 1. The location of the first network and the receiver heights.

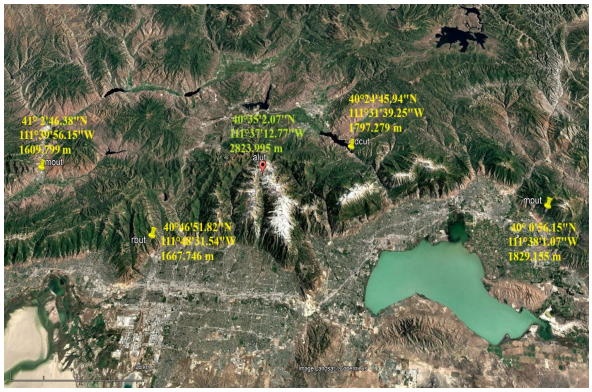

Figure 2. The location of the second network and the receiver heights.

The coordinates of the stations are given in Tables 1 and 2.

Station ID	Latitude	Longitude	height
es12	32°43'0.00"N	51°37'58.00" E	1592.727 m
es13	32°36'52.00"	51°36'58.00"	1634.344 m
	N	E	
es14	32°42'38.00" N	51°43'28.00" E	1565.116 m
ejlas	32°35'30.00" N	51°44'44.00" E	1578.326 m
Central receiver	32°36'55.23" N	51°39'22.44" E	1714.912 m

Table 1. the coordinates of the stations in the first network.

Station ID	Latitude	Longitude	height
dcut	40°24'45.94" N	111°31'39.25" W	1797.279 m
mout	41° 2'46.38"N	111°39'56.15" W	1609.799 m
mput	40° 0'56.15"N	111°38'1.07"W	1829.155 m
rbut	40°46'51.82" N	111°48'31.54" W	1667.746 m
Central receiver	40°35'2.07"N	111°37'12.77" W	2823.995 m

Table 2. the coordinates of the stations in the second network.

3. Accuracy Assessment of Tropospheric Delay Interpolation in the Networks

in order to investigate the accuracy of ZTD interpolation, we determined zenith tropospheric delays for all stations by processing GNSS observations using CSRS-PPP (Canadian Spatial Reference System – Precise Point Positioning) online service. It should be noted that ZTD values obtained by PPP processing have an accuracy of about 2 mm to 5 mm (Dousa and Bennitt. 2013) and are enough accurate for this study. Then we used the equations (1) and (2) introduced in (Wubbena et al., 1996; Varner, 2000) for interpolation of tropospheric delay.

$$T = ax + by + c \quad (1)$$

$$T = ax + by + ch + d \quad (2)$$

in these equations T is the ZTD values, x and y are the coordinates of receiver and h is the height of receiver. After estimating the coefficients a, b, c and d by least squares estimation and using the ZTD values of surrounding receivers as observations, we compute the interpolated ZTD values for the location of central receiver in a 3000 seconds time period. In order to evaluate the ZTD interpolation accuracy we compute the Root Mean Square Error (RMSE) using the equation (3).

$$RMSE = \sqrt{\sum_{k=1}^{N} \frac{(T - T_i)^2}{N}} \quad (3)$$

In this equation T is the ZTD values obtained by PPP processing and T_i is the ZTD values obtained by interpolation, k

index is related to the epoch number and N is total number of the epochs. After the computations we found that the amount of RMSE using the equations (1) and (2) is 30 mm and 28 mm respectively in the first network and in the second network is 259 mm and 272 mm. for a better comparison, Figure 3 show interpolation RMSE for the both networks and interpolation equations. The blue bar in this figure is related to equation (1) and the yellow bar is related to equation (2).

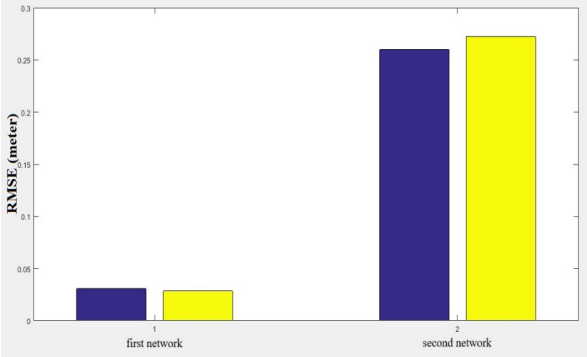

Figure 3. ZTD interpolation RMSE using equation (1) (blue bar) and equation (2) (yellow bar)

As it is seen in the figure, it is obvious that the interpolation in the first network significantly is more accurate in comparison with the second network. height difference between the central and surrounding receivers in the second network caused a large interpolation error.

4. Error Analysis

Several studies have demonstrated that within dense GNSS networks, the interpolation error of the Zenith Tropospheric Delay remains almost equivalent to the original uncertainty of the estimated ZTD values at the reference stations. Typically, when the inter-station spacing is less than about 20–30 km, ZTD interpolation using linear or geostatistical models (e.g., kriging) results in errors of approximately 3–5 mm RMS, which are comparable to the accuracy of ZTD derived from PPP or network-based solutions. According to (Champollion et al. 2009) and (Dousa and Bennitt 2013), spatial variations of ZTD over short horizontal scales are relatively smooth, and thus interpolation within the network introduces only minor additional uncertainty. Similarly, (Li et al. 2014) and (Bock et al. 2013) confirmed that the interpolation error inside the network generally remains within a few millimeters, whereas it increases significantly when extrapolating beyond the network boundaries or in sparse GNSS configurations.

5. Improving the Accuracy of ZTD Interpolation

In the third section we saw that the height difference between the rover and reference stations in the second network caused a large interpolation error. Given that the height directly effects on the dry component of tropospheric delay and this component forms approximately 90 percent of total delay, we can conclude that the interpolation error in the second network is related to dry component. So, in this section we are going to introduce a new method to improve the accuracy of zenith tropospheric delay interpolation. Based on this method, we eliminate the dry part of tropospheric delay from the total zenith delay and we add a modified dry component By theoretically transferring the surrounding receivers to the elevation of the central receiver. To compute the dry part of ZTD values we use equation (4) that is known as saastamoinen model (Krueger et al. 2004).

$$T_h = 0.0022768 \frac{P_0}{1 - 0.00266\cos(2\varphi) - 0.00000028 h_0} \quad (4)$$

Where P_0 is Surface pressure in [hPa], φ is Ellipsoidal latitude and h_0 is Surface height above the ellipsoid in [km]. We can determine the surface pressure as a function of height according to the equation (5) (Böhm et al., 2006).

$$P_0 = 1013.25\,(1 - 0.0000226\,h_0)^{5.225} \quad (5)$$

After computing the dry component, the wet component can be obtained by subtracting the dry part from the total delay as below:

$$T_w = T - T_h \quad (6)$$

To compute the modified dry component for the surrounding receivers, we substitute the latitude of surrounding receivers and the height of central receiver in equations (4) and (5). after computing the modified dry component, we add it to the wet part and we compute a modified ZTD for the surrounding receivers as a consequent. These steps can be summarized in the equation (7).

$$T_{modified} = T - 0.0022768 \frac{1013.25\,(1-0.0000226\,h_s)^{5.225}}{1-0.00266\cos(2\varphi_s)-0.00000028\,h_s} + \\ +0.0022768 \frac{1013.25\,(1 - 0.0000226\,h_c)^{5.225}}{1 - 0.00266\cos(2\varphi_c) - 0.00000028 h_c} \quad (7)$$

Where T is the ZTD, $T_{modified}$ is the modified ZTD, φ_s is the ellipsoidal latitude of surrounding receiver, h_s is the height of surrounding receiver and h_c is the height of the central receiver. after repeating the interpolation process using modified ZTD values, the computed RMSE of interpolation in the first network is 16 mm and 28 mm using equation (1) and (2) respectively. These amounts are 21 mm and 29 mm for the second network. Figure 4 and Figure 5 show the interpolation RMSE using standard and modified methods for both of the networks and both of the interpolation equations. The yellow bar in these figures is related to the modified method. For better review, some parameters like the minimum interpolation error, maximum interpolation error and mean interpolation error are given in Table 3.

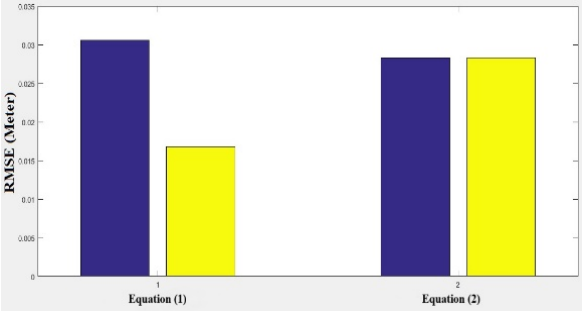

Figure 4. ZTD interpolation RMSE in the first network before and after using modified method.

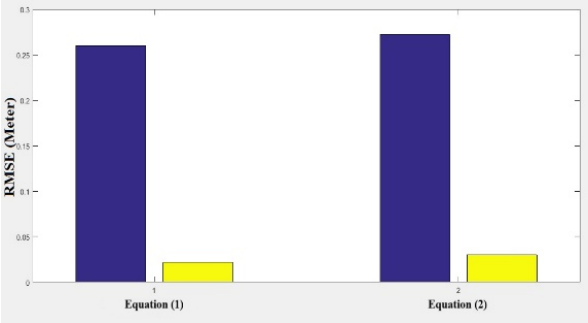

Figure 5. ZTD interpolation RMSE in the second network before and after using modified method.

Network Number	Equation Number	Interpolation Method	Min Error (mm)	Max Error (mm)	Mean Error (mm)
1	1	Standard	0	94	28
		Modified	0	72	11
	2	Standard	0	119	19
		Modified	0	119	19
2	1	Standard	217	277	259
		Modified	0	38	21
	2	Standard	216	309	272
		Modified	0	65	29

Table 2. Interpolation parameters using the standard and modified algorithms.

As it is seen in the figures, the accuracy of interpolation in both of the networks and for both of the interpolation equations increases after using proposed method. This increase in accuracy was 46% and 92% at best for the equation (1) in the first and second network respectively. In addition, analysing the error parameters given in the Table 2 shows that applying modified algorithm with the equation (1), has the best performance in interpolation for both of the networks.

6. Conclusion

This study evaluated the impact of elevation differences on the accuracy of tropospheric delay interpolation for InSAR applications using GNSS-derived ZTD data. The results clearly indicate that interpolation errors increase significantly when the elevation difference between reference and target stations grows. To address this limitation, a modified approach based on the Saastamoinen model was developed to compensate for the dry component of the troposphere at differing altitudes. By theoretically transferring the dry component to a uniform elevation level, the interpolation accuracy improved by up to 92% in networks with large height variations. The proposed method provides a practical and computationally efficient enhancement for InSAR tropospheric delay corrections, particularly in regions with complex topography. Future work could integrate real-time atmospheric modeling or machine learning approaches to further refine the interpolation accuracy and extend the applicability of this method to large-scale InSAR monitoring systems.

References

Amelung, F., Yun, S.-H., Walter, T. R., Segall, P., Kim, S.-W., 2007. Stress Control of Deep Rift Intrusion at Mauna Loa Volcano, Hawaii. Science, 316, 1026–1030.

Bawden, G. W., Thatcher, W., Stein, R. S., Hudnut, K. W., Peltzer, G., 2001. Tectonic contraction across Los Angeles after removal of groundwater pumping effects. Nature, 412, 812–815.

Bekaert, D. P. S., Hooper, A., Wright, T. J., 2015. A spatially variable power law tropospheric correction technique for InSAR data. Journal of Geophysical Research: Solid Earth, 120, 1345–1356.

Bekaert, D. P. S., Walters, R. J., Wright, T. J., Hooper, A. J., Parker, D. J., 2015. Statistical comparison of InSAR tropospheric correction techniques. Remote Sensing of Environment, 170, 40–47.

Bell, J. W., Amelung, F., Henry, C. D., 2012. InSAR analysis of the 2008 Reno-Mogul earthquake swarm: Evidence for westward migration of Walker Lane style dextral faulting. Geophysical Research Letters, 39, L18306

Berardino, P., Fornaro, G., Lanari, R., Sansosti, E., 2002. A new algorithm for surface deformation monitoring based on small baseline differential SAR interferograms. IEEE Transactions on Geoscience and Remote Sensing, 40(11), 2375–2383.

Bock, O., Bosser, P., Pacione, R., Nuret, M., Fourrié, N., Parracho, A., 2013. A high-quality reprocessed ground-based GPS dataset for atmospheric process studies, radiosonde and model evaluation, and reanalysis of climate. Geoscientific Data Journal, 1(2), 105–122.

Cao, Y., Jónsson, S., Li, Z., 2021. Advanced InSAR tropospheric corrections from global atmospheric models that incorporate spatial stochastic properties of the troposphere. Journal of Geophysical Research: Solid Earth, 126(5).

Cao, Y., Li, Z., Wei, J., Hu, J., Duan, M., Feng, G., 2017. Stochastic modeling for time series InSAR: with emphasis on atmospheric effects. Journal of Geodesy, 92(2), 185–204.

Cao, Y., Li, Z., Amelung, F., 2019. Mapping ground displacement by a multiple phase difference-based InSAR approach: With stochastic model estimation and turbulent troposphere mitigation. Journal of Geodesy.

Cao, Y., Li, Z., Wei, J., Hu, J., Duan, M., Feng, G., 2017. Stochastic modeling for time series InSAR: with emphasis on atmospheric effects. Journal of Geodesy, 92(2), 185–204.

Cavalié, O., & Jónsson, S., 2014. Block-like plate movements in eastern Anatolia observed by InSAR. Geophysical Research Letters, 41, 26–31.

Champollion, C., Masson, F., Bouin, M. N., Walpersdorf, A., Chéry, J., Doerflinger, E., 2009. GPS water vapor tomography: Preliminary results from the ESCOMPTE field experiment. Atmospheric Research, 94(3), 470–480.

Delacourt, C., Briole, P., Achache, J. A., 1998. Tropospheric corrections of SAR interferograms with strong topography. Application to Etna. Geophysical Research Letters, 25(15), 2849–2852.

Doin, M.-P., Lasserre, C., Peltzer, G., Cavalié, O., Doubre, C., 2009. Corrections of stratified tropospheric delays in SAR interferometry: Validation with global atmospheric models. Journal of Applied Geophysics, 69(1), 35–50.

Dousa, J., Bennitt, G.V., 2013. Estimation and evaluation of hourly updated global GPS Zenith Total Delays over ten months. GPS Solut 17, 453–464.

Elliott, J. R., Biggs, J., Parsons, B., Wright, T. J., 2008. InSAR slip rate determination on the Altyn Tagh Fault, northern Tibet, in the presence of topographically correlated atmospheric delays. Geophysical Research Letters, 35. L12309.

Fattahi, H., Amelung, F., 2015. InSAR bias and uncertainty due to the systematic and stochastic tropospheric delay. Journal of Geophysical Research: Solid Earth, 120(12), 8758–8773.

Feng, G., Hetland, E. A., Ding, X., Li, Z., Zhang, L., 2010. Coseismic fault slip of the 2008 Mw 7.9 Wenchuan earthquake estimated from InSAR and GPS measurements. Geophysical Research Letters, 37. L01302.

Ferretti, A., Prati, C., Rocca, F., 2001. Permanent Scatterers in SAR Interferometry. IEEE Transactions on Geoscience and Remote Sensing, 39(1), 8–20.

Foster, J., Brooks, B., Cherubini, T., Shacat, C., Businger, S., Werner, C. L., 2006. Mitigating atmospheric noise for InSAR using a high resolution weather model. Geophysical Research Letters, 33, L16304.

Hobiger, T., Kinoshita, Y., Shimizu, S., Ichikawa, R., Furuya, M., Kondo, T., Koyama, Y., 2010. On the importance of accurately ray-traced troposphere corrections for Interferometric SAR data. Journal of Geodesy, 84(9), 537–546.

Hooper, A., 2008. A multi-temporal InSAR method incorporating both persistent scatterer and small baseline approaches. Geophysical Research Letters, 35, L16302.

Houlie, N., Funning, G. J., Burgmann, R., 2016. Use of a GPS-Derived Troposphere Model to Improve InSAR Deformation Estimates in the San Gabriel Valley, California. IEEE Transactions on Geoscience and Remote Sensing, 54(9), 5365–5374.

Jolivet, R., Grandin, R., Lasserre, C., Doin, M. P., Peltzer, G., 2011. Systematic InSAR tropospheric phase delay corrections from global meteorological reanalysis data. Geophysical Research Letters, 38, L17311.

Jónsson, S., 2008. Importance of post-seismic viscous relaxation in southern Iceland. Nature Geoscience, 1(2), 136–139.

Jónsson, S., Segall, P., Pedersen, R., & Björnsson, G., 2003. Post-earthquake ground movements correlated to pore-pressure transients. Nature, 424, 179–183.

Krueger E., Schuler T., Hein G.W., Martellucci A., Blarzino G., 2004. Galileo tropospheric correction approaches developed within GSTB-V1. In: Proceedings of ENC-GNSS 2004, Rotterdam, The Netherlands, 16–19 May.

Li, Z., Cao, Y., Wei, J., Duan, M., Wu, L., Hou, J., Zhu, J., 2019. Time-series InSAR ground deformation monitoring: Atmospheric delay modeling and estimating. Earth-Science Reviews, 192, 258–284.

Li, Z. W., Ding, X. L., Liu, G. X., 2004. Modeling atmospheric effects on InSAR with meteorological and continuous GPS observations: algorithms and some test results. Journal of Atmospheric and Solar-Terrestrial Physics, 66(11), 907–917.

Li, Z., Fielding, E. J., Cross, P., 2009. Integration of InSAR Time-Series Analysis and Water-Vapor Correction for Mapping Postseismic Motion After the 2003 Bam (Iran) Earthquake. IEEE Transactions on Geoscience and Remote Sensing, 47(9), 3220–3230.

Li, Z. W., Xu, W. B., Feng, G. C., Hu, J., Wang, C. C., Ding, X. L., & Zhu, J. J., 2012. Correcting atmospheric effects on InSAR with MERIS water vapor data and elevation-dependent interpolation model. Geophysical Journal International, 189(2), 13.

Li, Z., 2005. Interferometric synthetic aperture radar (InSAR) atmospheric correction: GPS, Moderate Resolution Imaging Spectroradiometer (MODIS), and InSAR integration. Journal of Geophysical Research, 110, B03410.

Liang, H., Zhang, L., Ding, X., Lu, Z., Li, X., 2018. Toward Mitigating Stratified Tropospheric Delays in Multitemporal InSAR: A Quadtre Aided Joint Model. IEEE Transactions on Geoscience and Remote Sensing, 1–13.

Lin, Y.-n. N., Simons, M., Hetland, E. A., Muse, P., DiCaprio, C., 2010. A multiscale approach to estimating topographically correlated propagation delays in radar interferograms. Geochemistry, Geophysics, Geosystems, 11, Q09002.

Liu, P., Li, Q., Li, Z., Hoey, T., Liu, G., Wang, C., 2016. Anatomy of Subsidence in Tianjin from Time Series InSAR. Remote Sensing, 8(3), 266.

Liu, S., Hanssen, R., Mika, Á., 2009. On the value of high-resolution weather models for atmospheric mitigation in SAR interferometry. Geoscience and Remote Sensing Symposium, 2009 IEEE International, IGARSS 2009, Vol. 2.

Li, X., Zhang, X., Ren, X., Fritsche, M., Wickert, J., Schuh, H., 2014. Precise positioning with current multi-GNSS constellations: GPS, GLONASS, Galileo and BeiDou. Journal of Geodesy, 89(6), 607–635.

Massonnet, D., Rossi, M., Carmona, C., Adragna, F., Peltzer, G., Feigl, K., Rabaute, T., 1993. The displacement field of the Landers earthquake mapped by Radar interferometry. Nature, 364(6433), 138–142.

Onn, F., Zebker, H. A., 2006. Correction for interferometric synthetic aperture radar atmospheric phase artifacts using time series of zenith wet delay observations from a GPS network. Journal of Geophysical Research, 111, B09102.

Onn, F., Zebker, H., 2006. Correction for interferometric synthetic aperture radar atmospheric phase artifacts using time series of zenith wet delay observations from a GPS network. Journal of Geophysical Research, 111(B9), B09102.

Plattner, C., Amelung, F., Baker, S., Govers, R., Poland, M., 2013. The role of viscous magma mush spreading in volcanic flank motion at Kīlauea Volcano, Hawai'i. Journal of Geophysical Research: Solid Earth, 118, 2474–2487.

Rivera, A. M. M., Amelung, F., Mothes, P., Hong, S.-H., Nocquet;, J.-M., Jarrin;, P., 2017. Ground deformation before the 2015 eruptionsof Cotopaxi volcano detected by InSAR. Geophysical Research Letters, 44, 6607–6615.

Ruch, J., Wang, T., Xu, W., Hensch, M., Jónsson, S., 2016. Oblique rift opening revealed by reoccurring magma injection in central Iceland. Nature Communications, 7(1).

Sandwell, D. T., Sichoix, L., 2000. Topographic phase recovery from stacked ERS interferometry and a low-resolution digital elevation model. Journal of Geophysical Research, 105(B12), 28211–28222.

Siddique, M. A., Strozzi, T., Hajnsek, I., Frey, O., 2018. A case study on the correction of atmospheric phases for SAR tomography in mountainous regions. IEEE Transactions on Geoscience and Remote Sensing, 57(1), 416–431.

Sigmundsson, F., Hreinsdóttir, S., Hooper, A., Árnadóttir, T., Pedersen, R., Roberts, M. J., 2010. Intrusion triggering of the 2010 Eyjafjallajökull explosive eruption. Nature, 468(7322), 426–430.

Simons, M., Fialko, Y., & Rivera, L., 2002. Coseismic Deformation from the 1999 Mw 7.1 Hector Mine, California, Earthquake as Inferred from InSAR and GPS Observations. Bulletin of the Seismological Society of America, 92(4), 1390–1402.

Varner, C. C., 2000. DGPS carrier phase networks and partial derivative algorithms: Calgary.

Wadge, G., Webley, P. W., James, I. N., Bingley, R., Dodson, A., Waugh, S., 2002. Atmospheric models, GPS and InSAR measurements of the tropospheric water vapor field over Mount Etna. Geophysical Research Letters, 29(19), 11-1–11-11.

Walters, R. J., Elliott, J. R., Li, Z., Parsons, B., 2013. Rapid strain accumulation on the Ashkabad fault (Turkmenistan) from atmosphere-corrected InSAR. Journal of Geophysical Research: Solid Earth, 118, 3674–3690.

Webley, P. W., Bingley, R. M., Dodson, A. H., Wadge, G., Waugh, S. J., James, I. N., 2002. Atmospheric water vapor correction to InSAR surface motion measurements on mountains: results from a dense GPS network on Mount Etna. Physics and Chemistry of the Earth, Parts A/B/C, 27(4–5), 363–370.

Wicks, C. W., 2002. Magmatic activity beneath the quiescent Three Sisters volcanic center, central Oregon Cascade Range, USA. Geophysical Research Letters, 29(7), 1122.

Wright, T. J., Parsons, B., England, P. C., Fielding, E. J., 2004. InSAR Observations of Low Slip Rates on the Major Faults of Western Tibet. Science, 305, 236–239.

Wubbena, G., Bagge, A., Seeber, G., Böder, V., Hankemeier, P., 1996. Reducing distance dependent errors for real-time precise DGPS applications by establishing reference station networks. Paper presented at the PROCEEDINGS OF ION GPS.

Yang, Z., Li, Z., Zhu, J., Yi, H., Hu, J., Feng, G., 2017. Deriving Dynamic Subsidence of Coal Mining Areas Using InSAR and Logistic Model. Remote Sensing, 9(2), 125.